

Geophysical Research Letters[®]



RESEARCH LETTER

10.1029/2024GL111033

Key Points:

- For the first time, a relationship between Ocean and Land Color Instrument and Global Navigation Satellite System is observed and defined
- An empirical retrieval model is proposed to directly derive high-temporal-resolution water vapor from Ocean and Land Color Instrument data
- The newly retrieved water vapor has satisfactory performance when compared with additional Global Navigation Satellite System measurements

Supporting Information:

Supporting Information may be found in the online version of this article.

Correspondence to:

Z. Liu,
lszzliu@polyu.edu.hk

Citation:

Xu, J., & Liu, Z. (2024). An observed relationship between satellite-estimated transmittance and ground-estimated water vapor: Implications for high-temporal-resolution water vapor retrieval from non-geostationary satellite measurements. *Geophysical Research Letters*, 51, e2024GL111033. <https://doi.org/10.1029/2024GL111033>

Received 25 JUN 2024

Accepted 13 SEP 2024

Author Contributions:

Conceptualization: Jiafei Xu, Zhizhao Liu

Data curation: Jiafei Xu

Formal analysis: Jiafei Xu

Funding acquisition: Zhizhao Liu

Investigation: Jiafei Xu

Methodology: Jiafei Xu

Project administration: Zhizhao Liu

Supervision: Zhizhao Liu



Validation: Jiafei Xu

Writing – original draft: Jiafei Xu

© 2024. The Author(s).

This is an open access article under the terms of the [Creative Commons Attribution-NonCommercial-NoDerivs License](#), which permits use and distribution in any medium, provided the original work is properly cited, the use is non-commercial and no modifications or adaptations are made.

An Observed Relationship Between Satellite-Estimated Transmittance and Ground-Estimated Water Vapor: Implications for High-Temporal-Resolution Water Vapor Retrieval From Non-Geostationary Satellite Measurements

Jiafei Xu¹  and Zhizhao Liu¹ 

¹Department of Land Surveying and Geo-Informatics, The Hong Kong Polytechnic University, Kowloon, Hong Kong, China

Abstract The magnitude of integrated water vapor (IWV) varies considerably in the spatial-temporal domain, which demonstrates the significance of high-spatiotemporal-resolution IWV observations for atmospheric water vapor distribution monitoring, both locally and globally. Unlike previously published algorithms based on data fusion, an empirical retrieval algorithm is for the first time proposed to directly retrieve high-temporal-resolution IWV estimates from near-infrared radiance observations of the non-geostationary Ocean and Land Color Instrument (OLCI). The retrieval algorithm is developed based on an observed regression relationship between satellite-based OLCI-estimated transmittance and ground-based Global Navigation Satellite System (GNSS)-estimated IWV in the temporal domain. The results show that all newly retrieved IWV estimates have an overall good consistency with ground-based IWV from additional GNSS-sensed measurements, indicating the feasibility of the retrieval approach. The performance of the retrieval algorithm is acceptable and satisfactory when compared with that of IWV retrievals listed in previous studies.

Plain Language Summary Integrated water vapor (IWV) is the largest natural greenhouse component, which plays a crucially important role in weather, climate, and other related fields. Remote sensing of IWV from satellite-based instruments provides a unique technique for monitoring atmospheric water vapor distribution at proper spatial and temporal resolutions in both local and global areas. However, non-geostationary satellite-retrieved IWV observations have much lower temporal resolutions compared to geostationary satellite-sensed IWV measurements. The previously published improvements in the temporal resolution of non-geostationary satellite-retrieved IWV estimates are primarily performed based on data fusion approaches using reanalysis-based high-temporal-resolution IWV data. We propose a feasible IWV retrieval algorithm for directly retrieving high-temporal-resolution IWV data from non-geostationary Ocean and Land Color Instrument (OLCI)-sensed near-infrared radiance observations. For the first time, this study provides implications for the direct retrieval of high-temporal-resolution IWV estimates from non-geostationary satellite measurements. The retrieval algorithm has significant potential to be applicable to other non-geostationary OLCI-like instruments, such as Medium Resolution Imaging Spectrometer (MERIS), Medium Resolution Spectral Imager (MERSI), and Moderate Resolution Imaging Spectroradiometer (MODIS).

1. Introduction

Water vapor is a crucial climatical parameter that plays a vital role in the hydrological cycle, atmospheric circulation, and energy budget (Ashcroft et al., 2016; Bojinski et al., 2014; Cess, 2005; Held & Soden, 2000; Sherwood et al., 2010). The magnitude of water vapor varies considerably in the spatiotemporal dimension (Trenberth et al., 2005), denoting the importance of accurate integrated water vapor (IWV) measurements with approximate spatial and temporal resolutions (Chen & Liu, 2016; Li & Long, 2020).

IWV can be observed from satellite-based and ground-based data (Vaquero-Martínez et al., 2018; Xu & Liu, 2022d). Ground-based IWV observations are frequently employed as IWV references to validate satellite-retrieved IWV estimates (Antón et al., 2015; Liu et al., 2006; Xu & Liu, 2022c). In particular, Global Navigation Satellite System (GNSS), can provide high-temporal-resolution IWV data, which are little affected by weather conditions (Vaquero-Martínez & Antón, 2021). For this reason, ground-based GNSS-measured IWV

Writing – review & editing: Zhizhao Liu

data have also been utilized to develop water vapor retrieval/calibration algorithms for satellite-sensed IWV observations (Vaquero-Martínez & Antón, 2021; Xu & Liu, 2022a, 2023b).

Remote sensing of IWV from satellite-based instruments yields a unique means for atmospheric water vapor distribution monitoring at an approximate spatiotemporal resolution in both local and global coverages (Vaquero-Martínez et al., 2018). IWV can be retrieved from satellite-sensed measurements using different spectral wavelengths like microwave, infrared (IR), and near-IR (Du et al., 2015; Lee et al., 2019; Xu & Liu, 2022b). In particular, near-IR IWV observations have been the most frequently used satellite water vapor products over the past several decades (He & Liu, 2019; Xu & Liu, 2023c). The Ocean and Land Color Instrument (OLCI) is a remote sensing instrument on-board the non-geostationary Sentinel-3 satellite series (Donlon et al., 2012). The OLCI-sensed operational IWV retrievals are calculated based on a 2-band ratio of radiances from a near-IR window channel at 885 nm (O18) and a near-IR IWV absorption channel at 900 nm (O19) (Bennartz & Fischer, 2001; Mertikas et al., 2020; Xu & Liu, 2021). The OLCI-derived cloud-free IWV data, in general, have an overall good agreement with GNSS-measured reference IWV estimates, with a root-mean-square error (RMSE) of 3 and 4 mm (Mertikas et al., 2020; Xu & Liu, 2022d).

However, non-geostationary satellite-derived IWV data, in general, have a relatively low temporal resolution in both regional and global areas (Li & Long, 2020; Peng et al., 2014), while geostationary satellite-sensed observations can exclusively provide high-temporal-resolution full-disk IWV retrievals locally (Wong et al., 2015; Yang et al., 2017). It is crucial to precisely measure and monitor the worldwide water vapor variability using non-geostationary satellite-sensed IWV observations, which demonstrates the significance of high-spatiotemporal-resolution IWV satellite measurements (Li & Long, 2020). The previous improvements in the temporal resolution of non-geostationary satellite-retrieved IWV measurements are primarily conducted by fusing reanalysis-based high-temporal-resolution IWV estimates (Li & Long, 2020; Wu et al., 2023; Zhang & Yao, 2021). For instance, Li and Long (2020) utilized an Enhanced Spatial and Temporal Adaptive Reflectance Fusion Model (ESTARFM) to enhance the spatiotemporal resolution of operational IWV retrievals from polar-orbiting Moderate Resolution Imaging Spectroradiometer (MODIS) near-IR observations based on reanalysis-based ERA5 IWV data. The results showed that the fused IWV data had improvements in accuracy and spatiotemporal-resolution compared to operational MODIS near-IR IWV observations (Li & Long, 2020).

Here, we observed an empirical relationship between measurements from OLCI and GNSS in the temporal domain. Then we used the empirical relationship function to retrieve high-temporal-resolution IWV satellite data, different from the previous research based on data fusion approaches. For the first time, this work provides insights into directly deriving high-temporal-resolution IWV estimates using near-IR radiance data from non-geostationary satellite-sensed observations.

2. Study Region and Data

The research region in this letter is chiefly located in Europe, with latitudes from 35°08' N to 62°23' N and longitudes from 9°40' W to 41°34' E (see Figure 1). The selection of Europe is primarily because there are quite a lot of ground-based GNSS stations that can be used in algorithm development and verification. Two-type data measurements from OLCI and GNSS, collected from 1 January 2019 to 31 December 2020 across Europe, are utilized.

OLCI is an imaging instrument on-board the polar-orbiting Sentinel-3A and Sentinel-3B satellites, which contains 21 channels in the spectra from 0.4 to 1.02 μm (Donlon et al., 2012). It is capable of covering the globe coverage every 2-day (Donlon et al., 2012). The local observation time of the Sentinel-3 satellites is frequently at $\sim 10:00$ a.m. (Donlon et al., 2012). In the European region, the Coordinated Universal Time (UTC) is approximate to the local time, with an overall difference of 1 and 2 hr. As a result, the Sentinel-3 OLCI observations are frequently at ~ 10 UTC in Europe, as demonstrated in Figure S1 in Supporting Information S1.

The OLCI-retrieved operational IWV estimates are calculated based on a 2-channel ratio approach by using radiance observations from a near-IR IWV absorption channel (O19; 900 nm) and a near-IR window channel (O18; 885 nm) (Bennartz & Fischer, 2001; Mertikas et al., 2020; Xu & Liu, 2021). In this letter, the operational OLCI Level-1 Full Resolution (OL_1_EFR) product is utilized, which has radiance estimates of each band of the OLCI sensor. The land quality and science flag data of the operational OLCI Level-2 Land Full Resolution (OL_2_LFR) product are utilized to define the sky conditions of OLCI-sensed radiance data. Both OL_1_EFR

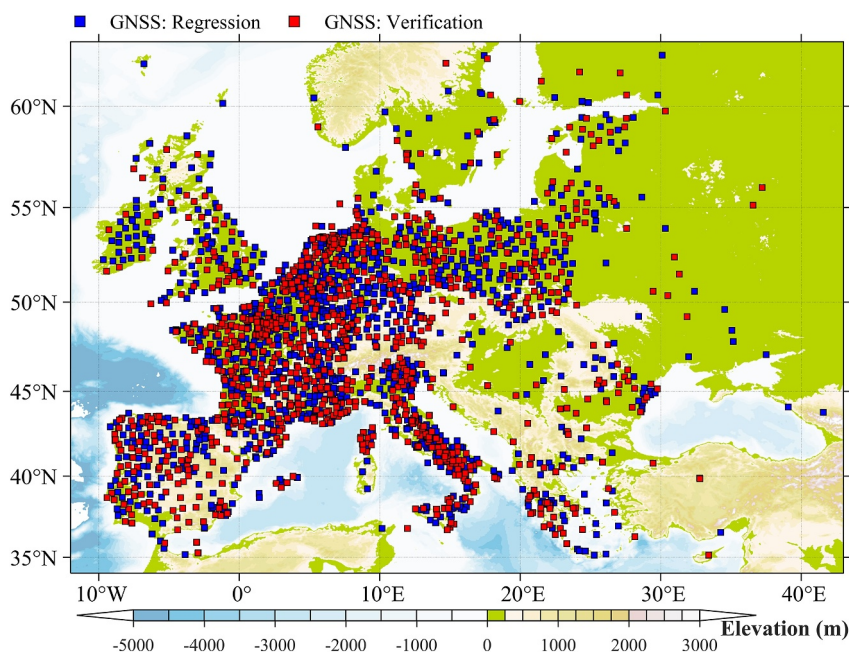


Figure 1. Research area and distributions of ground-based GNSS stations. The blue squares indicate GNSS stations employed for regression analysis between observations from OLCI and GNSS, while the red squares indicate GNSS stations employed for the verification of newly derived IWV estimates. The color bar indicates the altitude of GNSS stations.

and OL_2_LFR products have a full spatial-resolution of 300 m. Only cloud-free OLCI-based radiance data are used in this letter, as clouds have a significant influence on satellite near-IR observations (He & Liu, 2019; Mertikas et al., 2020; Xu & Liu, 2022c).

Additionally, ground-based IWV, collected from 1,186 GNSS stations in 2019 across Europe (blue squares in Figure 1), is utilized for the empirical regression analysis between observations from OLCI and GNSS. On the other hand, IWV data, measured from additional 1,089 GNSS stations in 2019–2020 over Europe (red squares in Figure 1), are employed to validate the performance of newly retrieved IWV estimates. All GNSS IWV data are obtained from the Nevada Geodetic Laboratory (Blewitt et al., 2018), which are determined from wet zenith delay observations based on Bevis et al. (1994, 1992).

In the regression procedure, OLCI-sensed measurements, closest to GNSS stations, are selected and utilized, provided that the closest distance between paired OLCI and GNSS observations does not exceed 5 km. In the temporal domain, we choose and use high-temporal-resolution hourly GNSS-sensed IWV data that are recorded on the same day as the OLCI-sensed data.

For the verification of newly derived IWV data, the temporal discrepancies between measurements from GNSS and OLCI must be the closest, in addition to the spatial collocation criterion utilized in the regression procedure. The spatiotemporal collocation criteria between GNSS and OLCI are based on the previous research (Vaquero-Martínez et al., 2018; Xu & Liu, 2023a).

3. Methodologies

3.1. Theoretical Basis

From space, remote sensing of radiance measurements from polar-orbiting OLCI near-IR spectra can be calculated as (Gao & Goetz, 1990):

$$L_s(\lambda) = \left(\frac{\mu E(\lambda)}{\pi} \right) T(\lambda) \rho(\lambda) + L_p(\lambda) \quad (1)$$

where $L_s(\lambda)$, $E(\lambda)$, $T(\lambda)$, $\rho(\lambda)$, and $L_p(\lambda)$ are the radiance, solar flux, transmittance, surface reflectance, and path radiance at the spectral wavelength λ , respectively; μ is the cosine of solar zenith angle. In the near-IR spectra, $L_p(\lambda)$ can be frequently ignored on account that the impact of aerosols on near-IR observations is limited (Kaufman & Gao, 1992). As a result, Equation 1 can be further re-written in a more simplified form as:

$$\rho^*(\lambda) = \frac{\pi L_s(\lambda)}{\mu E(\lambda)} = T(\lambda)\rho(\lambda) \quad (2)$$

where $\rho^*(\lambda)$ is the apparent reflectance at the spectral wavelength λ (Kaufman & Gao, 1992).

Surface reflectance varies considerably in different types of surfaces; hence, it is impossible to estimate the atmospheric transmittance using radiance data of one individual near-IR absorption channel of the OLCI sensor (Bennartz & Fischer, 2001; Kaufman & Gao, 1992; Schläpfer et al., 1998). In the operational OLCI IWV retrieval algorithm, a 2-band ratio approach is presented to derive the atmospheric transmittance based on two near-IR channels, namely O19 at 900 nm (i.e., absorption band) and O18 at 885 nm (i.e., window band) (Bennartz & Fischer, 2001; Xu & Liu, 2021). Additionally, previous studies indicated that the retrieval performance of 2-band ratio approach is comparable to that of 3-band ratio method (He & Liu, 2020; Wang et al., 2021; Xu & Liu, 2022b). For these reasons, a 2-band ratio approach is used in this work to determine the transmittance of the O19 900-nm IWV absorption channel of the OLCI sensor. It is calculated as (Bennartz & Fischer, 2001; Xu & Liu, 2021):

$$T(900 \text{ nm}) = \frac{\rho^*(900 \text{ nm})}{\rho^*(885 \text{ nm})} = \frac{R(900 \text{ nm})}{R(885 \text{ nm})} \quad (3)$$

where $T(900 \text{ nm})$ is the transmittance in the OLCI O19 900-nm IWV absorption channel; $\rho^*(900 \text{ nm})$ is the apparent reflectance in the OLCI O19 900-nm IWV absorption channel; $\rho^*(885 \text{ nm})$ is the apparent reflectance in the OLCI O18 885-nm non-absorption channel; $R(900 \text{ nm})$ and $R(885 \text{ nm})$ are the radiances measured from O19 and O18 bands of the OLCI sensor, respectively.

3.2. Relationship Between Satellite-Based OLCI-Estimated Transmittance and Ground-Based GNSS-Estimated Water Vapor in the Temporal Domain

Figure 2 shows the scatterplots of the regression relationship between OLCI-based transmittance and GNSS-based IWV from 00 to 23 UTC, which is performed based on the data of 2019 across Europe. In this regression analysis, the collocated OLCI–GNSS data points, which have a distance that is more than three standard deviations of the mean, are removed and not used. For each hour, 54,916 data pairs are used to examine the relationship between observations from OLCI and GNSS instruments in the temporal domain, that is, 00 to 23 UTC.

It can be observed in Figure 2 that the satellite-based OLCI-estimated transmittances have an overall strong correlation with ground-based GNSS-measured IWV at different UTC hours, with a correlation coefficient (CC) from -0.95 to -0.83 . The CC decreases with the increase of the time difference between OLCI and GNSS measurements. In particular, the strength of the correlation relationship (i.e., CC) between OLCI and GNSS is the highest when the regression time is approximate to the OLCI observation time (i.e., ~ 10 UTC). It is thus plausible that IWV retrievals at different hours throughout a specific day have an overall significant correlation with the OLCI-sensed data obtained during the OLCI observation time on that same day. Consequently, we can use one “instantaneous” OLCI-sensed transmittance data observation to retrieve “continuous” high-temporal-resolution IWV data on the same day.

After testing several types of regression functions, an exponential function is chosen to define the empirical relationship between satellite-based OLCI-estimated transmittance and ground-based GNSS-estimated IWV in the temporal domain. For each hour, this relationship can be defined as:

$$T(900 \text{ nm}) = a \exp(bW) + c \exp(dW) \quad (4)$$

where W is the IWV; a , b , c , and d are the coefficients of the regression function, respectively. The coefficients a , b , c , and d are calculated based on the least-squares fitting approach.

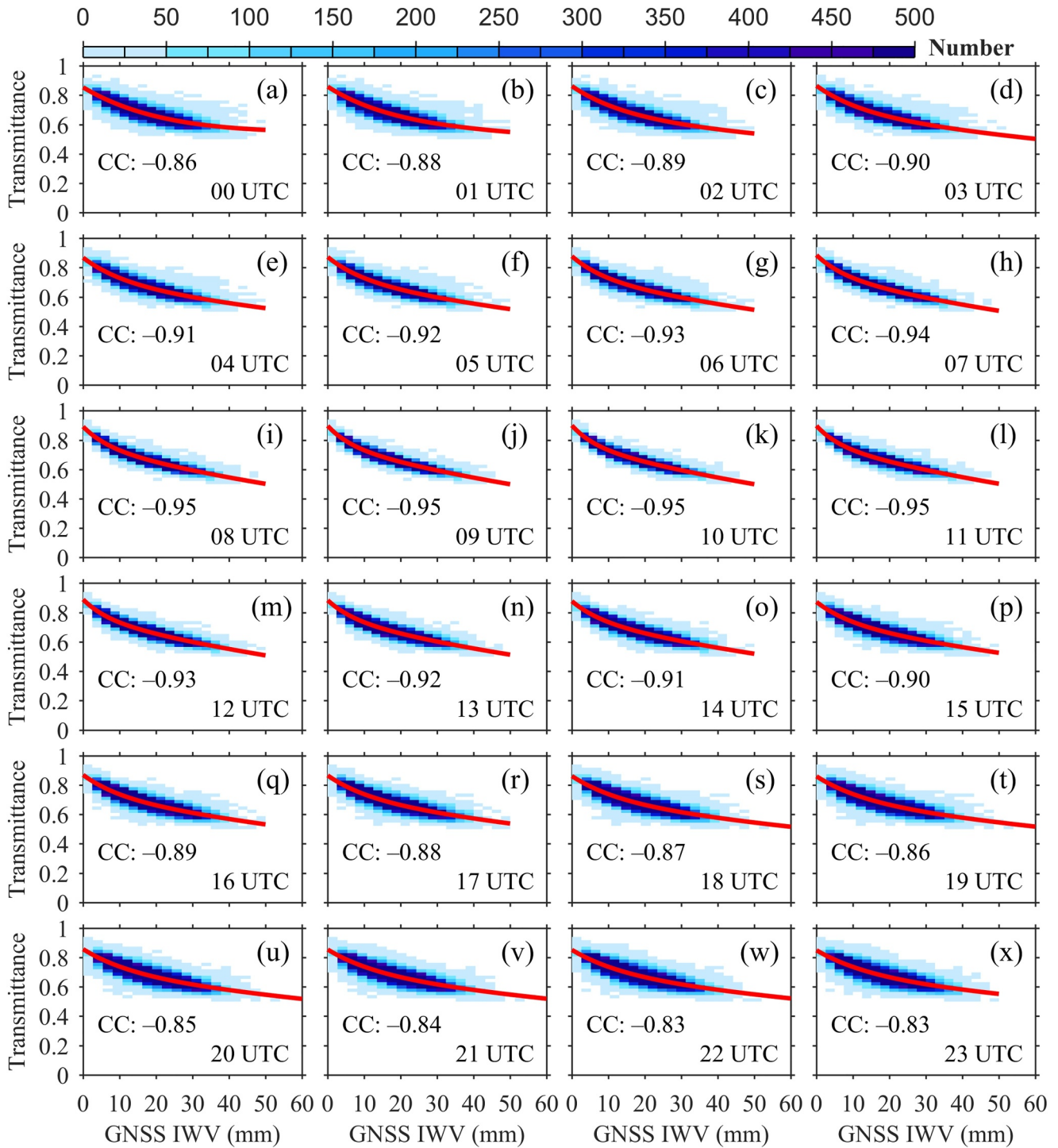


Figure 2. Scatter plots of the relationship between 2-band ratio transmittances from the O19 900-nm bands channel of the OLCI sensor and IWV from GNSS observations in the temporal domain, based on collocated OLCI–GNSS data in 2019 across Europe. (a)–(x): 00, 01, 02, 03, 04, 05, 06, 07, 08, 09, 10, 11, 12, 13, 14, 15, 16, 17, 18, 19, 20, 21, 22, and 23 UTC, respectively.

3.3. Retrieval of High-Temporal-Resolution IWV From OLCI-Sensed Radiance Observations

Table S1 in Supporting Information S1 summarizes the coefficients a , b , c , and d of the regression function $T(900\text{ nm}) = a \exp(bW) + c \exp(dW)$ from 00 to 23 UTC, which are determined using collocated OLCI–GNSS data in 2019 over Europe. The calculation of coefficients of the empirical fitting function relies significantly upon the

regression data set; hence, different regression data could obtain different coefficients. The least-squares fitting results of coefficients a , b , c , and d for four independent subsets of regression data are listed in Table S2 in Supporting Information S1. It can be measured in Table S2 in Supporting Information S1 that the regression coefficients vary slightly for different regression data sets. Additionally, the regression coefficients listed in Table S2 in Supporting Information S1 are very consistent with those shown in Table S1 in Supporting Information S1. Overall, our least-squares fitting parameters of the exponential function are reliable and consistent for the regression data in 2019 over Europe.

Once the coefficients are determined, high-temporal-resolution hourly IWV retrievals can be estimated from polar-orbiting OLCI-sensed radiance data based on Equations 3 and 4. The verification of newly retrieved IWV data is conducted using ground-based IWV from additional 1,089 GNSS stations during 2019–2020 across Europe, which is independent of regression data from 1,186 GNSS stations in 2019 over Europe. Four assessment factors, that is, CC, RMSE, standard deviation (STD), and mean bias (MB), are utilized, which are calculated as:

$$CC = \frac{\sum_{i=1}^N (W_O - \bar{W}_O)(W_R - \bar{W}_R)}{\sqrt{\sum_{i=1}^N (W_O - \bar{W}_O)^2 (W_R - \bar{W}_R)^2}} \quad (5)$$

$$RMSE = \sqrt{\frac{1}{N} \sum_{i=1}^N (W_O - W_R)^2} \quad (6)$$

$$STD = \sqrt{\frac{1}{N} \sum_{i=1}^N (W_O - W_R)^2 - \left(\frac{1}{N} \sum_{i=1}^N (W_O - W_R) \right)^2} \quad (7)$$

$$MB = \frac{1}{N} \sum_{i=1}^N (W_O - W_R) \quad (8)$$

where W_O is newly derived IWV estimates from polar-orbiting OLCI near-IR observations; \bar{W}_O is the average of newly derived IWV estimates from polar-orbiting OLCI near-IR observations; W_R is reference IWV estimates from GNSS observations; \bar{W}_R is the average of reference IWV estimates from GNSS observations; N is the total count of paired measurements for the verification of newly retrieved IWV data.

4. Results and Discussion

By using coefficients listed in Table S1 in Supporting Information S1, high-temporal-resolution IWV data (i.e., hourly) are retrieved from non-geostationary OLCI-sensed radiance measurements during 2019–2020 over Europe. Figure 3 lists the overall verification result of newly derived hourly IWV estimates from the OLCI instrument, by conducting comparisons with GNSS-observed reference IWV data.

The new OLCI-derived IWV estimates had an overall good consistency with reference IWV from GNSS observations, with CC, RMSE, STD, and MB of 0.87, 4.23, 4.22, and 0.19 mm, respectively. In 2019, the newly retrieved IWV data presented CC = 0.87, RMSE = 4.25 mm, STD = 4.25 mm, and MB = 0.15 mm compared to GNSS-measured IWV estimates. The verification metrics of newly derived IWV observations in 2020 were similar to those in 2019, that is, CC = 0.86, RMSE = 4.20 mm, STD = 4.19 mm, and MB = 0.22 mm. This implies that the newly proposed retrieval algorithm is capable and stable in deriving high-temporal-resolution hourly IWV estimates from non-geostationary OLCI data, although the coefficients of the retrieval algorithm are calculated based on the data of 2019.

In Figure 3, the newly derived IWV retrievals also exhibited a good consistency with ground-based GNSS IWV measurements at different hours between 00 and 23 UTC. The CC between IWV from OLCI and GNSS was in the range of 0.79 (23 UTC) to 0.94 (09 and 10 UTC), with an RMSE between 2.59 mm (09 and 10 UTC) and 6.23 mm (23 UTC). At the same time, the new OLCI-retrieved IWV data showed an STD from 2.52 mm (09 UTC) to 6.15 mm (23 UTC) and an MB from −0.59 mm (11 UTC) to 0.98 mm (23 UTC), compared to GNSS-estimated

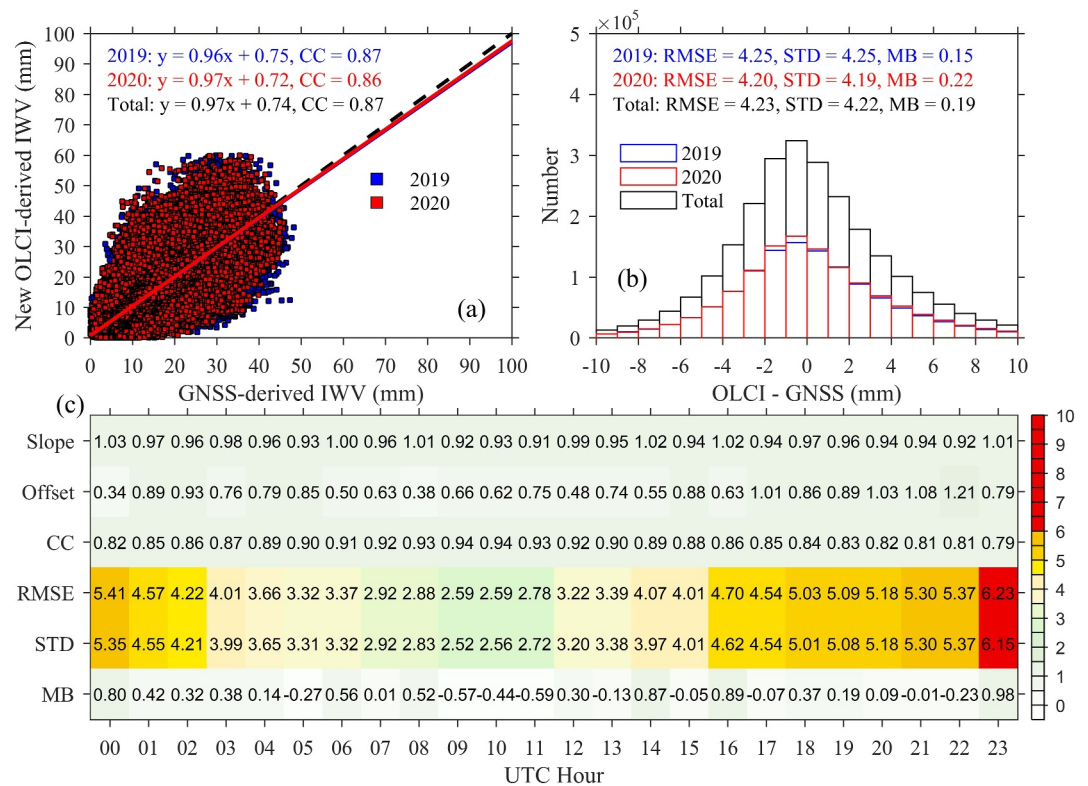


Figure 3. Verification of newly retrieved IWV data from the OLCI sensor using ground-based IWV from GNSS observations during 2019–2020 over Europe. (a): Scatter plot of hourly IWV from OLCI and GNSS; (b): Histogram of IWV differences between OLCI and GNSS; (c): Heatmap of slope, offset, CC, RMSE, STD, and MB of OLCI IWV versus GNSS IWV between 00 and 23 UTC.

IWV data. In terms of CC, RMSE, and STD, the retrieval algorithm had the highest IWV retrieval performance when the retrieval time was approximate to the OLCI observation time over Europe, that is, ~10 UTC. That is, the performance of OLCI IWV retrievals tended to degrade with the increment of differences between the retrieval time and OLCI observation time. This had a good consistency with the regression results shown in Figure 2.

The operational MODIS near-IR and IR IWV retrievals had an RMSE between 4 and 6 mm compared with GNSS IWV estimates (He & Liu, 2019; Xu & Liu, 2023c). For the operational OLCI water vapor product, it had an RMSE from 3 to 4 mm (Mertikas et al., 2020; Xu & Liu, 2022d, 2023a). It is thus summarized that the retrieval accuracy of our newly derived IWV estimates in terms of RMSE was comparable to that of operational MODIS and OLCI IWV retrievals. Additionally, our OLCI IWV retrievals had an RMSE of 2.59 mm around the OLCI observation time (i.e., ~10 UTC), which was better than operational OLCI IWV retrievals (RMSE = 3 and 4 mm). As shown in Figure S2 in Supporting Information S1, the performance of our newly derived IWV data in terms of RMSE was also better than that of the operational OLCI IWV retrievals. This further confirmed the effectiveness and practicality of our newly proposed retrieval approach. However, it should be mentioned that, in terms of STD, the newly retrieved IWV data exhibited poorer performance compared to the operational IWV data. Our newly retrieved IWV data also had slightly poorer performance than the fused IWV estimates shown in the previous work (Li & Long, 2020; Wu et al., 2023; Zhang & Yao, 2021). The overall retrieval accuracy of our OLCI-derived IWV data is acceptable and satisfactory when compared to that of IWV estimates in previous studies.

In addition, we also investigated the retrieval performance of newly derived IWV estimates in both temporal and spatial dimensions, with the results listed in Figure 4. Temporally, the daily mean IWV of newly derived IWV data showed an overall good consistency with that of reference GNSS-derived IWV estimates. In the spatial domain, the new IWV retrievals also had an overall good agreement with ground-based IWV from almost all GNSS stations over Europe. In particular, when the retrieval time was approximate to the OLCI measurement time, the RMSE and STD values were frequently below 3 mm in almost all GNSS stations. On the contrary, the

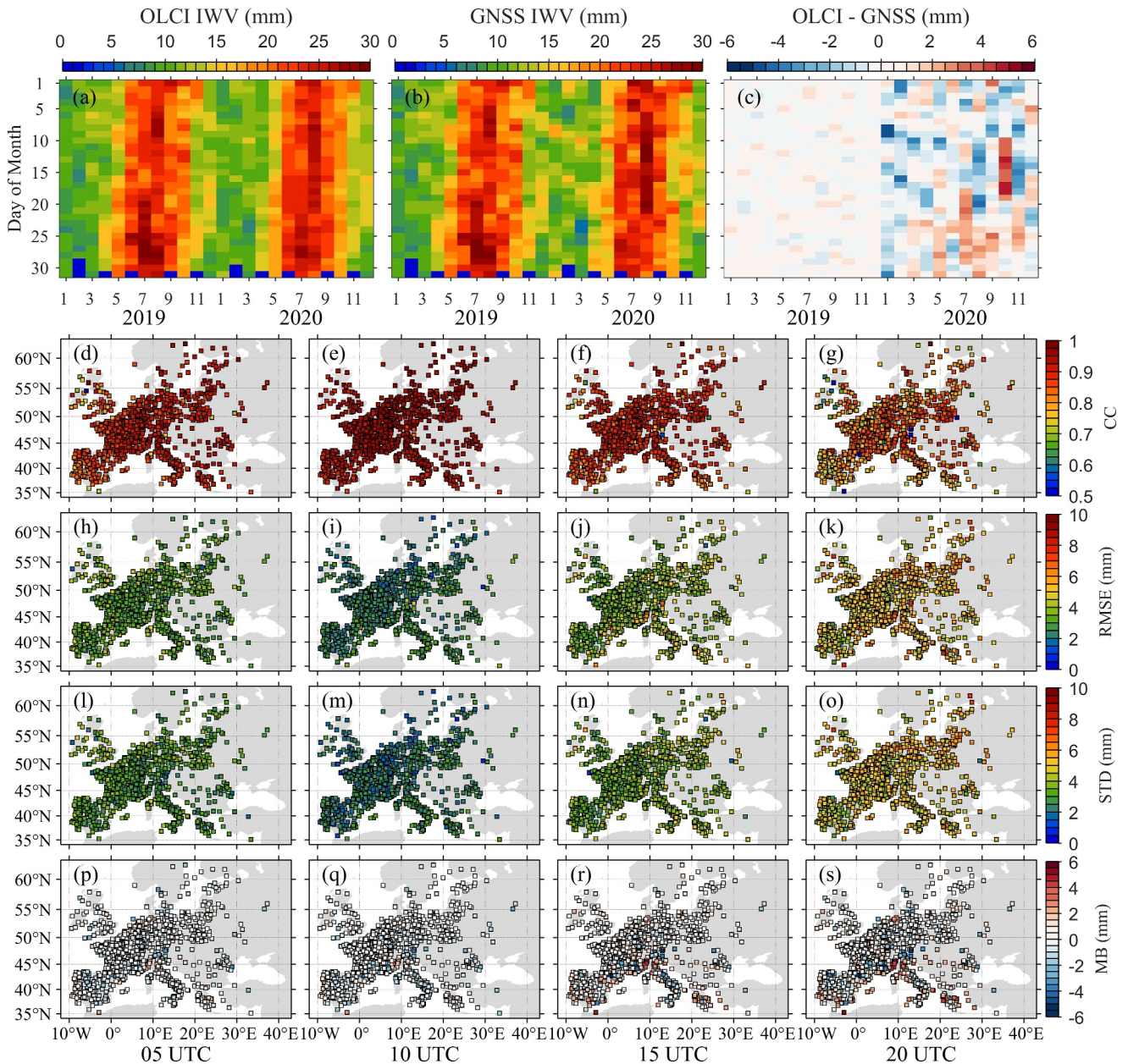


Figure 4. Spatiotemporal verification of newly retrieved IWB data from the OLCI sensor using ground-based IWB from GNSS observations during 2019–2020 over Europe. (a): Daily mean IWB from GNSS observations; (b): Daily mean IWB of newly derived IWB retrievals from the OLCI sensor; (c): Daily mean IWB differences between OLCI and GNSS; (d)–(g): CC between IWB from OLCI and GNSS at 05, 10, 15, and 20 UTC, respectively. (h)–(k): RMSE between IWB from OLCI and GNSS at 05, 10, 15, and 20 UTC, respectively. (l)–(o): STD between IWB from OLCI and GNSS at 05, 10, 15, and 20 UTC, respectively. (p)–(s): MB between IWB from OLCI and GNSS at 05, 10, 15, and 20 UTC, respectively.

station-wise verification metrics were relatively poor when the retrieval time was far from the OLCI observation time, that is, 23 UTC. This was consistent with the hourly verification metrics listed in Figure 3.

5. Conclusions

In this letter, an empirical relationship between measurements from OLCI and GNSS is observed and defined for the first time, which is feasible to be employed to directly retrieve high-temporal-resolution IWB estimates from polar-orbiting OLCI-sensed observations. This study offers initial insights into deriving high-temporal-resolution

IWV estimates from near-IR measurements of non-geostationary satellite instruments, differing from the previous research that typically uses data fusion methods.

It is found that all newly retrieved IWV data have an overall good consistency with ground-based GNSS-observed IWV estimates, denoting the feasibility and effectiveness of the empirical retrieval algorithm. The retrieval performance of newly derived IWV estimates in 2020 is comparable to that in 2019, which demonstrates the capability and stability of the newly developed retrieval algorithm. The retrieval algorithm exhibits the best IWV retrieval performance when the retrieval time is approximate to the OLCI observation time, that is, ~ 10 UTC. The retrieval performance of our OLCI-estimated IWV data degrades with the increase of differences between the retrieval time and OLCI observation time. The retrieval approach shows acceptable and satisfactory performance when compared with the accuracy of IWV data shown in previous studies.

Our IWV retrieval method is developed in the European region, and the performance of the retrieval approach is expected to be relatively suboptimal in other regions worldwide if directly applied using coefficients calculated in Europe. This is primarily because the UTC of satellite observations varies significantly from place to place across the globe, although their local observation times are consistent. Additionally, regional disparities in atmospheric conditions, such as temperature, humidity, and pressure, can significantly affect the accuracy of IWV retrievals in regions outside Europe when using European-determined coefficients. This is because atmospheric conditions can vary considerably between different regions, which can affect the coefficient calculation of the empirical retrieval algorithm. Hence, the coefficients of the retrieval algorithm, determined in the European region, could not be ideally suited for other regions worldwide, frequently resulting in suboptimal IWV retrievals due to regional differences in UTC observation times and atmospheric conditions.

In non-European regions, it is thus recommended to re-calculate the coefficients of the empirical retrieval algorithm using collocated OLCI–GNSS data pairs from these specific regions. Through this approach, we can tailor the coefficients to the unique UTC observation times and atmospheric conditions presented in the target regions, thereby optimizing the retrieval algorithm's performance for non-geostationary Sentinel-3 OLCI measurements in these specific areas. By accounting for regional differences in UTC observation times and atmospheric conditions, this coefficient adjustment significantly enhances the retrieval algorithm's capability to derive accurate high-temporal-resolution IWV data across various global regions. Ultimately, this will improve the overall accuracy and reliability of the retrieval algorithm, ensuring its effectiveness in diverse geographical contexts.

Given the significant impact of clouds on satellite-sensed near-infrared data, we exclusively utilize cloud-free OLCI radiance data in the development of our empirical IWV retrieval approach. As such, our algorithm is specifically intended for clear sky conditions and is not applicable in cloudy conditions. In future research, we plan to enhance the applicability of our retrieval approach to cloudy conditions by integrating parameters associated with cloud properties and characteristics. In addition, we will continue to refine the retrieval approach to further improve its retrieval performance in the temporal domain, which could involve incorporating additional data sources and exploring new techniques.

Data Availability Statement

The Sentinel-3 OLCI data can be freely obtained from the CREODIAS at <https://explore.creodias.eu/>. The GNSS IWV data can be freely accessed from the Nevada Geodetic Laboratory at http://geodesy.unr.edu/gps_timeseries/trop/ (Blewitt et al., 2018).

References

- Antón, M., Loyola, D., Román, R., & Vömel, H. (2015). Validation of GOME-2/MetOp-A total water vapour column using reference radiosonde data from the GRUAN network. *Atmospheric Measurement Techniques*, 8(3), 1135–1145. <https://doi.org/10.5194/amt-8-1135-2015>
- Ashcroft, L., Gergis, J., & Karoly, D. J. (2016). Long-term stationarity of El Niño–Southern Oscillation teleconnections in southeastern Australia. *Climate Dynamics*, 46(9), 2991–3006. <https://doi.org/10.1007/s00382-015-2746-3>
- Bennartz, R., & Fischer, J. (2001). Retrieval of columnar water vapour over land from backscattered solar radiation using the Medium Resolution Imaging Spectrometer. *Remote Sensing of Environment*, 78(3), 274–283. [https://doi.org/10.1016/S0034-4257\(01\)00218-8](https://doi.org/10.1016/S0034-4257(01)00218-8)
- Bevis, M., Businger, S., Chiswell, S., Herring, T., Anthes, R., Rocken, C., & Ware, R. (1994). Gps meteorology—Mapping zenith wet delays onto precipitable water. *Journal of Applied Meteorology*, 33(3), 379–386. [https://doi.org/10.1175/1520-0450\(1994\)033<0379:GMMZWD>2.0.CO;2](https://doi.org/10.1175/1520-0450(1994)033<0379:GMMZWD>2.0.CO;2)
- Bevis, M., Businger, S., Herring, T. A., Rocken, C., Anthes, R. A., & Ware, R. H. (1992). GPS meteorology: Remote sensing of atmospheric water vapor using the global positioning system. *Journal of Geophysical Research*, 97(D14), 15787–15801. <https://doi.org/10.1029/92JD01517>

Acknowledgments

We gratefully thank the support from the Research Grants Council of Hong Kong under projects PolyU/RGC 15221620/B-Q80Q, 15205821/B-Q84W, and 15212622/B-Q94L. We would also like to thank the CREODIAS and Nevada Geodetic Laboratory for offering OLCI and GNSS measurements, respectively.

- Blewitt, G., Hammond, W. C., & Kreemer, C. (2018). Harnessing the GPS data explosion for interdisciplinary science. *Eos*, 99(10.1029), 485. <https://doi.org/10.1029/2018eo104623>
- Bojinski, S., Verstraete, M., Peterson, T. C., Richter, C., Simmons, A., & Zemp, M. (2014). The concept of essential climate variables in support of climate research, applications, and policy. *Bulletin of the American Meteorological Society*, 95(9), 1431–1443. <https://doi.org/10.1175/bams-d-13-00047.1>
- Cess, R. D. (2005). Water vapor feedback in climate models. *Science*, 310(5749), 795–796. <https://doi.org/10.1126/science.1119258>
- Chen, B., & Liu, Z. (2016). Global water vapor variability and trend from the latest 36 year (1979 to 2014) data of ECMWF and NCEP reanalyses, radiosonde, GPS, and microwave satellite. *Journal of Geophysical Research: Atmospheres*, 121(19), 11442–11462. <https://doi.org/10.1002/2016JD024917>
- Donlon, C., Berruti, B., Buongiorno, A., Ferreira, M.-H., Féménias, P., Frerick, J., et al. (2012). The global monitoring for environment and security (GMES) Sentinel-3 mission. *Remote Sensing of Environment*, 120, 37–57. <https://doi.org/10.1016/j.rse.2011.07.024>
- Du, J., Kimball, J. S., & Jones, L. A. (2015). Satellite microwave retrieval of total precipitable water vapor and surface Air temperature over land from AMSR2. *IEEE Transactions on Geoscience and Remote Sensing*, 53(5), 2520–2531. <https://doi.org/10.1109/TGRS.2014.2361344>
- Gao, B.-C., & Goetz, A. F. (1990). Column atmospheric water vapor and vegetation liquid water retrievals from airborne imaging spectrometer data. *Journal of Geophysical Research*, 95(D4), 3549–3564. <https://doi.org/10.1029/jd095i04p03549>
- He, J., & Liu, Z. (2019). Comparison of satellite-derived precipitable water vapor through near-infrared remote sensing channels. *IEEE Transactions on Geoscience and Remote Sensing*, 57(12), 10252–10262. <https://doi.org/10.1109/tgrs.2019.2932847>
- He, J., & Liu, Z. (2020). Water vapor retrieval from MODIS NIR channels using ground-based GPS data. *IEEE Transactions on Geoscience and Remote Sensing*, 58(5), 3726–3737. <https://doi.org/10.1109/TGRS.2019.2962057>
- Held, I. M., & Soden, B. J. (2000). Water vapor feedback and global warming. *Annual Review of Energy and the Environment*, 25(1), 441–475. <https://doi.org/10.1146/annurev.energy.25.1.441>
- Kaufman, Y. J., & Gao, B.-C. (1992). Remote sensing of water vapor in the near IR from EOS/MODIS. *IEEE Transactions on Geoscience and Remote Sensing*, 30(5), 871–884. <https://doi.org/10.1109/36.175321>
- Lee, Y., Han, D., Ahn, M.-H., Im, J., & Lee, S. J. (2019). Retrieval of total precipitable water from Himawari-8 AHI data: A comparison of random forest, extreme gradient boosting, and deep neural network. *Remote Sensing*, 11(15), 1741. <https://doi.org/10.3390/rs11151741>
- Li, X., & Long, D. (2020). An improvement in accuracy and spatiotemporal continuity of the MODIS precipitable water vapor product based on a data fusion approach. *Remote Sensing of Environment*, 248, 111966. <https://doi.org/10.1016/j.rse.2020.111966>
- Liu, J., Liang, H., Sun, Z., & Zhou, X. (2006). Validation of the Moderate-Resolution Imaging Spectroradiometer precipitable water vapor product using measurements from GPS on the Tibetan Plateau. *Journal of Geophysical Research*, 111(D14), D14103. <https://doi.org/10.1029/2005JD007028>
- Mertikas, S., Partinivelos, P., Tripolitsiotis, A., Kokolakis, C., Petrakis, G., & Frantzis, X. (2020). Validation of Sentinel-3 OLCI integrated water vapor products using regional GNSS measurements in Crete, Greece. *Remote Sensing*, 12(16), 2606. <https://doi.org/10.3390/rs12162606>
- Peng, S., Tang, B.-H., Wu, H., Tang, R., & Li, Z.-L. (2014). Estimating of the total atmospheric precipitable water vapor amount from the Chinese new generation polar orbit FengYun meteorological satellite (FY-3) data. In *2014 IEEE Geoscience and Remote Sensing Symposium* (pp. 3029–3032). <https://doi.org/10.1109/IGARSS.2014.6947115>
- Schläpfer, D., Borel, C. C., Keller, J., & Itten, K. I. (1998). Atmospheric precorrected differential absorption technique to retrieve columnar water vapor. *Remote Sensing of Environment*, 65(3), 353–366. [https://doi.org/10.1016/S0034-4257\(98\)00044-3](https://doi.org/10.1016/S0034-4257(98)00044-3)
- Sherwood, S. C., Roca, R., Weckwerth, T. M., & Andronova, N. G. (2010). Tropospheric water vapor, convection, and climate. *Reviews of Geophysics*, 48(2), RG2001. <https://doi.org/10.1029/2009RG000301>
- Trenberth, K. E., Fasullo, J., & Smith, L. (2005). Trends and variability in column-integrated atmospheric water vapor. *Climate Dynamics*, 24(7–8), 741–758. <https://doi.org/10.1007/s00382-005-0017-4>
- Vaquero-Martínez, J., & Antón, M. (2021). Review on the role of GNSS meteorology in monitoring water vapor for atmospheric Physics. *Remote Sensing*, 13(12), 2287. <https://doi.org/10.3390/rs13122287>
- Vaquero-Martínez, J., Antón, M., de Galisteo, J. P. O., Cachorro, V. E., Álvarez-Zapatero, P., Román, R., et al. (2018). Inter-comparison of integrated water vapor from satellite instruments using reference GPS data at the Iberian Peninsula. *Remote Sensing of Environment*, 204, 729–740. <https://doi.org/10.1016/j.rse.2017.09.028>
- Wang, L., Hu, X., Xu, N., & Chen, L. (2021). Water vapor retrievals from near-infrared channels of the advanced medium resolution spectral imager instrument onboard the Fengyun-3D satellite. *Advances in Atmospheric Sciences*, 38(8), 1351–1366. <https://doi.org/10.1007/s00376-020-0174-8>
- Wong, M. S., Jin, X., Liu, Z., Nichol, J. E., Ye, S., Jiang, P., & Chan, P. W. (2015). Geostationary satellite observation of precipitable water vapor using an empirical orthogonal function (EOF) based reconstruction technique over Eastern China. *Remote Sensing*, 7(5), 5879–5900. <https://doi.org/10.3390/rs70505879>
- Wu, J., Xia, L., Chan, T. O., Awange, J., Yuan, P., Zhong, B., & Li, Q. (2023). A novel fusion framework embedded with zero-shot super-resolution and multivariate autoregression for precipitable water vapor across the continental Europe. *Remote Sensing of Environment*, 297, 113783. <https://doi.org/10.1016/j.rse.2023.113783>
- Xu, J., & Liu, Z. (2021). Radiance-based retrieval of total water vapor content from sentinel-3A OLCI NIR channels using ground-based GPS measurements. *International Journal of Applied Earth Observation and Geoinformation*, 104, 102586. <https://doi.org/10.1016/j.jag.2021.102586>
- Xu, J., & Liu, Z. (2022a). A back propagation neural network-based algorithm for retrieving all-weather precipitable water vapor from MODIS NIR measurements. *IEEE Transactions on Geoscience and Remote Sensing*, 60, 1–14. <https://doi.org/10.1109/TGRS.2022.3219405>
- Xu, J., & Liu, Z. (2022b). Enhanced all-weather precipitable water vapor retrieval from MODIS near-infrared bands using machine learning. *International Journal of Applied Earth Observation and Geoinformation*, 114, 103050. <https://doi.org/10.1016/j.jag.2022.103050>
- Xu, J., & Liu, Z. (2022c). Evaluation of precipitable water vapor product from MODIS and MERSI-II NIR channels using ground-based GPS measurements over Australia. *IEEE Journal of Selected Topics in Applied Earth Observations and Remote Sensing*, 15, 8744–8758. <https://doi.org/10.1109/JSTARS.2022.3211879>
- Xu, J., & Liu, Z. (2022d). The first validation of Sentinel-3 OLCI integrated water vapor products using reference GPS data in Mainland China. *IEEE Transactions on Geoscience and Remote Sensing*, 60, 1–17. <https://doi.org/10.1109/TGRS.2021.3099168>
- Xu, J., & Liu, Z. (2023a). A Back Propagation neural network-based calibration approach for Sentinel-3 OLCI near-infrared water vapor product. *IEEE Geoscience and Remote Sensing Letters*, 20, 1–5. <https://doi.org/10.1109/LGRS.2023.3235983>
- Xu, J., & Liu, Z. (2023b). A gradient boosting decision tree based correction model for AIRS infrared water vapor product. *Geophysical Research Letters*, 50(14), e2023GL104072. <https://doi.org/10.1029/2023GL104072>

- Xu, J., & Liu, Z. (2023c). Water vapour products from ERA5, MERSI-II/FY-3D, OLCI/Sentinel-3A, OLCI/Sentinel-3B, MODIS/Aqua and MODIS/Terra in Australia: A comparison against in situ GPS water vapour data. *Quarterly Journal of the Royal Meteorological Society*, *149*(753), 1435–1458. <https://doi.org/10.1002/qj.4467>
- Yang, J., Zhang, Z., Wei, C., Lu, F., & Guo, Q. (2017). Introducing the new generation of Chinese geostationary weather satellites, Fengyun-4. *Bulletin of the American Meteorological Society*, *98*(8), 1637–1658. <https://doi.org/10.1175/BAMS-D-16-0065.1>
- Zhang, B., & Yao, Y. (2021). Precipitable water vapor fusion based on a generalized regression neural network. *Journal of Geodesy*, *95*(3), 36. <https://doi.org/10.1007/s00190-021-01482-z>